Journal of Engineering Mathematics **43:** 367–384, 2002.

The numerical modelling of a two-dimensional local exhaust system associated with an inclined jet flow

X. WEN[1], D. B. INGHAM[2] and B. FLETCHER[3]
[1]*School of the Environment, University of Leeds, Leeds, LS2 9JT, UK*
[2]*Department of Applied Mathematics, University of Leeds, Leeds, LS2 9JT, UK*
[3]*Health and Safety Executive, Broad Lane, Sheffield S3 7HQ, UK*

Received 4 September 2001; accepted in revised form 4 April 2002

Abstract. Previous mathematical models employed by the authors have been further developed in order to consider the effect of an inclined jet on the air flow of a two-dimensional bench-slot Aaberg exhaust system. The air flow in this local exhaust ventilation system is solved using two approaches, namely, (i) a simple potential-flow model and seeking the solution of the resulting Laplace equation by means of a boundary-integral technique, and (ii) a turbulent model using the k-ϵ formulation and solving the resulting turbulent Navier-Stokes equations by means of a control-volume method and the SIMPLE algorithm. The effect of the angle α that the jet makes with the direction of the surface of the workbench and the momentum ratio on the air flow in the exhaust system are investigated. It is found that, by inclining the jet, the system can become more energy efficient and the region of capture of the contaminant from close to the bench can be increased.

Key words: Aaberg exhaust system, boundary-integral method, control-volume method, potential flow, turbulent flow

1. Introduction

Many industrial processes result in the emission of contaminants, such as noxious gases, vapours, dust or heat, which may affect the quality of the indoor air. Breathing this polluted air may harm the health and well-being of the work people, create distressing working conditions and lead to a reduction in productivity. Local ventilation systems are used in many industries and are designed to remove the contaminant from a region close to the source(s) of the generation by the withdrawal of the air and the contaminant.

Traditional local exhaust hoods remove the air (in most situations both clear and polluted air) by only sucking the air into the ventilation system through the opening of the exhaust hood. In such ventilation systems the movement of the air in a ventilated space is limited as air flows towards the opening of the exhaust hood evenly from all directions, even from behind the exhaust hood. This results in a sharp decrease in the air velocity with increasing distance from the exhaust opening, namely the air speed reduces inversely with distance from the opening in a two-dimensional system and as the square of the distance from the opening in a three-dimensional system. Thus, the polluted air may escape capture if the air flow induced by the hood is weaker than the air flow induced by diffusion, buoyancy or background disturbances. Further, when using exhaustion (suction) alone, considerable energy may be required to induce sufficient air speeds to ensure capture of the pollutant. By using a jet it is possible to create a jet-induced flow which restricts the air being withdrawn to a small region of space in front of the hood and in this region the air speed towards the exhaust hood is significantly increased.

The combination of the exhaustion and the injection is the principle behind the Aaberg exhaust hood and this system is capable of creating controlled air movements towards the exhaust opening over far greater distances than is possible by the use of exhaustion alone. Thus, in comparison with the traditional exhaust hoods, the Aaberg exhaust system can significantly improve the capture efficiency of the hood.

In the last two decades some experimental and theoretical research has been performed in order to explore the advantage of the Aaberg principle and the focus of this research has been mainly on two types of exhaust hoods, namely, circular and slot workbench hoods. Experimental investigations and analyses on the Aaberg exhaust systems with a circular hood have been performed by Høgsted [1], Hyldgard [2], Pedersen and Nielsen [3] and Fletcher Saunders [4, 5]. Braconnier *et al.* [6] conducted experiments on an Aaberg workbench, a slot hood, and reported that the capture efficiency is 1·5 to 3·7 times higher than that obtained when using only a conventional exhaust system. Pedersen [7] also reported an experimental investigation on the flow created by an Aaberg slot exhaust hood. He reported that the enhancement of the surface air velocity on the workbench induced by the Aaberg slot exhaust hood is similar to that along the centre-line of the circular Aaberg exhaust hood he had previously tested. Pedersen [7] also found that the capture efficiency may be about three times higher than the conventional slot exhaust system. In order to encourage industrial application of the Aaberg principle, a further experimental investigation has been performed by Sprecher and Weber [8]. In these experiments the direction of the jet flow is perpendicular, *i.e.* at an angle of 90°, to the direction of the suction.

For the jet direction at an angle of 90°, Hunt and Ingham [9] have employed a combination of analytical and numerical solutions of the governing mathematical equations to model the air flow of the Aaberg hood. A theoretical model was developed for the axisymmetrical fluid flow of the Aaberg exhaust hood by Hunt and Ingham [9, 10] and Hunt [11] in which they produced the solution for the air flow by developing an analysis of the turbulent boundary layer, the turbulent jet and the air flow due to the jet. They obtained the exhaust flow outside the boundary layer using a potential-flow model. This simple potential model was extended to analyze the two-dimensional air flow of the Aaberg slot exhaust hood by Hunt [11]; Hunt and Ingham [12] and Wen and Ingham [13] have made a further development of the potential-flow model to include a more complex geometry of the two-dimensional Aaberg exhaust system. In all these configurations, detailed comparisons between the potential model and the full turbulent k-ϵ model have shown that they are both in very good agreement with the experimental measurements.

For the two-dimensional Aaberg exhaust system, Wen *et al.* [14] have developed the earlier potential-flow model, using a boundary-integral technique, in order to include the situation where the jet direction is not at 90° to the main suction velocity. Hunt *et al.* [15] and Wen and Ingham [16] have revealed that the performance of jet-assisted hoods may be enhanced considerably if the angle between the initial jet direction and the suction direction is less than 90°. Further, Gubler and Moser [17] have employed a CFD technique to simulate the air flow around a circular Aaberg hood in the presence of an inclined jet flow. When the momentum ratio I is fixed at $I = 0{\cdot}82$, their numerical results revealed that the capture distance increases as the angle α decreases, provided that the jet flow does not collapse and form a short circuit into the exhaust flow.

In this paper the boundary-integral technique for the potential-flow model, as developed by Wen *et al.* [14], and the control-volume method for the turbulent-flow model are used to predict the air flow for a two-dimensional Aaberg slot workbench hood with an inclined

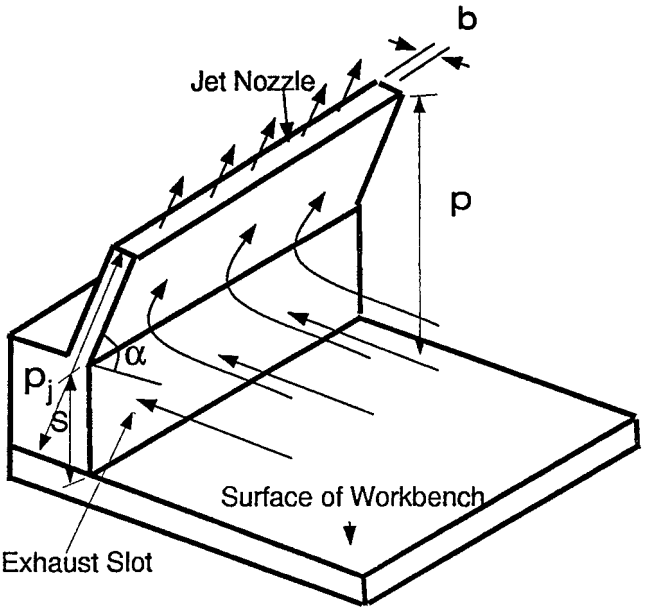

Figure 1. A three-dimensional schematic diagram of the Aaberg slot exhaust hood.

jet flow. A comparison of the numerical results produced by these two models shows good agreement and the results reveal a significant increase in the air velocity close to the surface of the workbench when the angle α is decreased, provided that the jet does not short-circuit.

2. Mathematical models

A schematic diagram of the Aaberg slot exhaust hood is shown in Figure 1. The system is operated by drawing air with an average velocity u_i through a slot which has a width S and injecting air with an average velocity u_j from the jet nozzle which has a width b; m_i is the flux of air per unit width withdrawn into the exhaust slot and m_j is the flux of fluid per unit width issued from the jet nozzle; α is the angle between the surface of the workbench and the central plane of the jet flow; p is the vertical distance from the jet nozzle to the surface of the workbench. Finally, p_j is the distance from the jet nozzle to the point where the extended central plane of the jet flow meets the extended workbench surface.

We assume that the width of the Aaberg slot is very large and, therefore, we consider only the flow pattern on its central plane, *i.e.* we assume a two-dimensional flow. In practice the contaminant is released from close to the surface of the workbench and this will be assumed to be the situation in this investigation. Further, it is assumed that the contaminant is neutrally-buoyant, which means that the existence of the contaminant in the flow field has no effect on the air flow. It is also assumed that the air flow is of constant density and steady. It should be noted that it is not necessary for the fluxes of fluid withdrawn into the exhaust slot, m_i, to be the same as those issued from the jet nozzle, m_j, and this flux of fluid must be matched by fluid entering, or exiting the system at large distances from the bench. In fact, in most experimental investigations, $m_i \neq m_j$.

2.1. THE TURBULENT-FLOW MODEL

In this paper we use a turbulent-flow model to simulate the two-dimensional steady and turbulent air flow for the Aaberg slot exhaust hoods. If the standard k-ϵ model, as developed by Launder and Spalding [17], is employed, the governing equations are the continuity equation:

$$\frac{\partial u}{\partial x} + \frac{\partial v}{\partial y} = 0, \tag{1}$$

and the momentum equations:

$$\frac{\partial(\rho uu)}{\partial x} + \frac{\partial(\rho vu)}{\partial y} = -\frac{\partial p}{\partial x} + \frac{\partial}{\partial x}(\mu_e \frac{\partial u}{\partial x}) + \frac{\partial}{\partial y}(\mu_e \frac{\partial u}{\partial y}), \tag{2}$$

$$\frac{\partial(\rho uv)}{\partial x} + \frac{\partial(\rho vv)}{\partial y} = -\frac{\partial p}{\partial y} + \frac{\partial}{\partial x}(\mu_e \frac{\partial v}{\partial x}) + \frac{\partial}{\partial y}(\mu_e \frac{\partial v}{\partial y}). \tag{3}$$

where ρ, u and v are the density and the x- and y-components of the air velocity, respectively, p is the pressure and μ_e is the turbulent viscosity which is computed using the following equations:
the turbulent kinetic-energy equation:

$$\frac{\partial(\rho uk)}{\partial x} + \frac{\partial(\rho vk)}{\partial y} = \frac{\partial}{\partial x}(\frac{\mu_e}{\sigma_k}\frac{\partial k}{\partial x}) + \frac{\partial}{\partial y}(\frac{\mu_e}{\sigma_k}\frac{\partial k}{\partial y}) + \Phi - \rho\epsilon, \tag{4}$$

the turbulent kinetic-energy dissipation equation:

$$\frac{\partial(\rho u\epsilon)}{\partial x} + \frac{\partial(\rho v\epsilon)}{\partial y} = \frac{\partial}{\partial x}(\frac{\mu_e}{\sigma_\epsilon}\frac{\partial \epsilon}{\partial x}) + \frac{\partial}{\partial y}(\frac{\mu_e}{\sigma_\epsilon}\frac{\partial \epsilon}{\partial y}) + C_1\frac{\epsilon}{k}\Phi - C_2\rho\frac{\epsilon^2}{k} \tag{5}$$

and

$$\mu_e = C_\mu \rho \frac{k^2}{\epsilon}, \tag{6}$$

where the quantities μ_e, k, ϵ and Φ are the turbulent viscosity, the turbulent kinetic-energy, the turbulent kinetic-energy dissipation and the turbulent generation, respectively.

The empirical constants chosen in all the calculations presented in this paper are as follows:

$$C_\mu = 0{\cdot}09, \quad C_1 = 1{\cdot}44, \quad C_2 = 1{\cdot}92, \quad \sigma_k = 1{\cdot}0, \quad \sigma_\epsilon = 1{\cdot}3. \tag{7}$$

These values for the constants are based on an extensive examination of different fluid flows, see for example Launder and Spalding [17], and they are widely used in numerous industrial applications.

The computational domain and the geometry of the exhaust system are shown in Figure 2. For such an irregular geometry, a body-fitted grid system is used to match the boundaries accurately and the control-volume method and the SIMPLE algorithm, see Patankar [20], are employed to obtain numerical solutions of the governing equations. At the exhaust slot and the jet nozzle, uniform velocities u_i and u_j are specified, whilst on solid surfaces the no-slip conditions of $u = v = 0$ are enforced. Because the velocity near the wall varies very rapidly, many grid points are needed in this region and this leads to a very expensive computation. However, this difficulty may be overcome by using the wall-function method, see Launder and

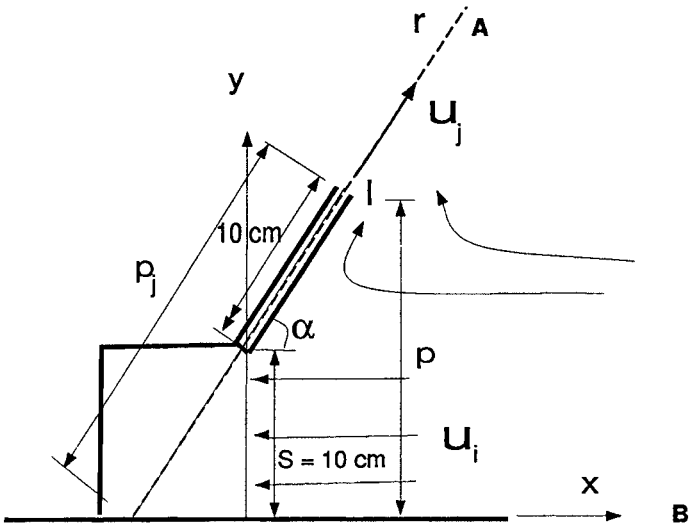

Figure 2. A two-dimensional schematic diagram of the Aaberg slot exhaust hood.

Spalding [18], which bridges the fully developed turbulent flow and the turbulent boundary-layer flow.

In all the results presented in this paper, the turbulence intensity at the jet nozzle is assumed to be 20% and at the inlet of the slot to be 10%. However, values for the turbulence intensities from 5% to 25% have been investigated, but all the results presented in this paper are almost independent of the values chosen in this range.

The open boundary of the solution domain is located at a sufficiently large distance from the exhaust system such that any further increase in the solution domain has a negligible effect on the flow pattern close to the exhaust system. On the open boundary, at a large distance from the Aaberg system, the boundary condition is imposed by enforcing the Bernoulli equation, namely,

$$p + \rho(u^2 + v^2)/2 = \text{ constant}. \tag{8}$$

This condition was found by Wen and Ingham [13] to produce accurate numerical results for the situation when $\alpha = 90°$.

2.2. THE POTENTIAL-FLOW MODEL

In previous numerical investigations, see for example Hunt and Ingham [9] and Wen and Ingham [13], into the air flow of the Aaberg exhaust system when the angle between the direction of the jet and the suction is 90°, it has been found that the potential-flow model provides an accurate solution for the air flow in comparison to both the turbulent-flow model and the experimental data. However, the potential-flow model is simpler and easier to employ than the turbulent model because it does not have the uncertainty in the determination of the boundary conditions on the open boundary or the difficulties in the numerical iterative procedure. Therefore, in this paper we also determine the numerical solution of the potential model using the boundary-integral technique as developed by Wen *et al.* [14] and therefore only points that are different to those described in that paper are highlighted here.

Under the assumption of two-dimensional, irrotational and inviscid fluid flow, the Navier-Stokes equation simplifies to the Laplace equation. Further, in order to simplify the geometry,

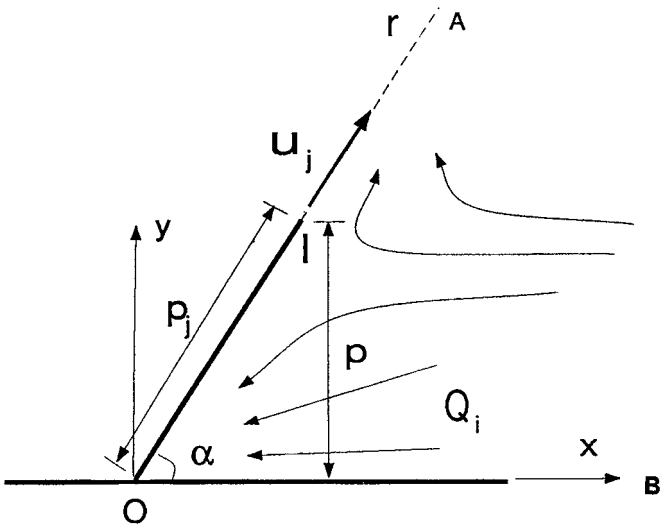

Figure 3. A two-dimensional schematic diagram of the Aaberg line sink exhaust hood.

we assume that the suction may be modelled as a line sink which is located on the surface of the workbench and Figure 3 shows a schematic diagram of the air flow. Under these assumptions, the solution of the potential air flow may be obtained by a combination of the potential flow induced by the jet and the potential flow into the sink which is located at the point O on the central plane of the jet and the surface of the workbench. It should be noted that it is not necessary to make these simplifying assumption on the geometry but, as we will show later, the results obtained from this model are sufficiently accurate without having to make the model more complex.

2.2.1. *Potential fluid flow induced by a jet*

When a turbulent jet emanates from a nozzle, the stream function ψ at the outer edge, or the 'boundary', is given by

$$\psi = A(r - p_j)^{1/2}, \tag{9}$$

where r and p_j are the distances from the points at the outer edge of the jet and the jet nozzle, respectively, to the line sink and the coefficient A is given by

$$A = Cu_j b^{1/2}, \tag{10}$$

where $C = 0{\cdot}31$ for a free jet.

The high-Reynolds-number flow from the nozzle is restricted to a narrow region but this jet flow induces motion of the air outside the jet. For simplicity, we assume that the jet has zero thickness so that the 'boundary' of the jet is at the outer edge of the line AI, see Figure 3, *i.e.* on the axis of the jet. From the stream function (9), the component of the air velocity U_n which is normal to the line AI, see Figure 3, is given by

$$U_n = \frac{1}{2}A(r - p_j)^{-1/2}. \tag{11}$$

A coordinate system (x, y) is introduced with the x-axis along OB and the y-axis vertically upwards from the origin at the point sink O. A boundary-integral equation for the horizontal component u on the boundary OA is given by (for more details see Wen *et al.* [14])

$$\frac{r_0^{\frac{\pi}{2\alpha}}}{\alpha}\int_0^{\infty}\frac{u(r)}{r^{\frac{\pi}{2\alpha}}(-r^{\frac{\pi}{2\alpha}}+r_0^{\frac{\pi}{2\alpha}})}\mathrm{d}r - u(r_0)\tan\alpha = b(r_0), \quad 0 \le r_0 \le \infty, \tag{12}$$

in which

$$b(r_0) = 0, \quad 0 \le r_0 \le p_j, \tag{13}$$

$$b(r_0) = \frac{A(r_0 - p_j)^{-1/2}}{2\cos\alpha}, \quad p_j \le r_0, \tag{14}$$

where r_0 is the distance of a general point on OA to the origin O. It should be noted that in Equations (12)–(14) the angle α is in radians, but in the section on Results and discussion and in all the figures the angle α is in degrees for the convenience of engineering applications, and the integral in Equation (12) extends to infinity because the solution domain is infinite.

In this paper we numerically solve the boundary-integral equation (12). The boundary OA is divided into N small elements and on each element a constant interpolation is employed when evaluating the integration in Equation (12). Clearly, we have to approximate the location of infinity in the integral ocurring in Equation (12). We have found that approximating infinity by $100p$ gives rise to results which do not graphically change by taking a larger value. Thus, in a similar manner to that employed in the conventional boundary-element method, the integrations over each interval may be performed analytically, including the intervals which contain the singularity point. Therefore the boundary-integral equation (12) is converted into a system of linear algebraic equations of the form

$$\sum_{i=1}^{N} a_{ij}u_i = b_j, \tag{15}$$

where u_i is the mean value of the horizontal component of the air velocity on the element i and we let η denote $-r^{\frac{\pi}{\alpha}}$ and use η_j to denote $-r_0^{\frac{\pi}{\alpha}}$. The coefficients in Equation (15) are given by

$$a_{ij} = \frac{1}{\pi}\left[\log\frac{\sqrt{-\eta_{i+1}}-\sqrt{-\eta_j}}{\sqrt{-\eta_i}-\sqrt{-\eta_j}} - \log\frac{\sqrt{-\eta_{i+1}}+\sqrt{-\eta_j}}{\sqrt{-\eta_i}+\sqrt{-\eta_j}}\right] \quad \text{when } \eta_{i+1} < \eta_j \quad \text{or } \eta_j < \eta_i, \tag{16}$$

$$a_{ij} = \frac{1}{\pi}\left[\log\frac{\sqrt{-\eta_{i+1}}-\sqrt{-\eta_j}}{\sqrt{-\eta_i}-\sqrt{-\eta_j}} - \log\frac{\sqrt{-\eta_{i+1}}+\sqrt{-\eta_j}}{\sqrt{-\eta_i}+\sqrt{-\eta_j}}\right] - \tan\alpha \quad \text{when } \eta_i < \eta_j < \eta_{i+1}, \tag{17}$$

$$b_j = 0 \qquad \text{when} \quad -p_j^{\frac{\pi}{\alpha}} < \eta_j < 0 \quad \text{or } 0 < r < p, \tag{18}$$

$$b_j = \frac{A[\,(-\eta_j)^{\frac{\alpha}{\pi}} - p_j\,]^{-1/2}}{2\cos\alpha} \qquad \text{when } \eta_j < -p_j^{\frac{\pi}{\alpha}} \quad \text{or } p_j < r_j, \tag{19}$$

where η_j is the midpoint of the boundary element and η_i and η_{i+1} are the end points of the boundary element. The linear system of algebraic equations (15) is solved by a Gaussian elimination procedure. Once the solution for the horizontal component of the air velocity on the boundary OI is found, the components of the air velocity in the solution domain are calculated by means of the expressions

$$u(x, y) = \frac{R^{\frac{\pi}{2\alpha}}}{\pi}[\, f(x, y)\sin(\frac{\pi}{2\alpha}\beta) + g(x, y)\cos(\frac{\pi}{2\alpha}\beta)\,], \tag{20}$$

$$v(x, y) = \frac{R^{\frac{\pi}{2\alpha}}}{\pi}[\, g(x, y)\sin(\frac{\pi}{2\alpha}\beta) - f(x, y)\cos(\frac{\pi}{2\alpha}\beta)\,], \tag{21}$$

where

$$R = \sqrt{x^2 + y^2}, \quad \beta = \arctan(y/x), \tag{22}$$

$$f(x, y) = f(R, \beta) = \int_{-\infty}^{0} \frac{u(\eta)[\eta - R^{\frac{\pi}{\alpha}} cos(\frac{\pi}{\alpha}\beta)]}{\sqrt{-\eta}\{\,[\eta - R^{\frac{\pi}{\alpha}}\cos(\frac{\pi}{\alpha}\beta)]^2 + [R^{\frac{\pi}{\alpha}}\sin(\frac{\pi}{\alpha}\beta)]^2\,\}}\mathrm{d}\eta \tag{23}$$

and

$$g(x, y) = g(R, \beta) = R^{\frac{\pi}{\alpha}}\sin(\frac{\pi}{\alpha}\beta)\int_{-\infty}^{0} \frac{u(\eta)}{\sqrt{-\eta}\{\,[\eta - R^{\frac{\pi}{\alpha}}\cos(\frac{\pi}{\alpha}\beta)]^2 + [R^{\frac{\pi}{\alpha}}\sin(\frac{\pi}{\alpha}\beta)]^2\,\}}\mathrm{d}\eta. \tag{24}$$

2.2.2. *Air flow due to the sink*
The complex velocity potential of the air flow induced by a line sink which is located at the point O is given by

$$u_s(z) - \mathrm{i}v_s(z) = -\frac{m_i}{\alpha}\frac{1}{z} \tag{25}$$

or

$$u_s(x, y) = -\frac{m_i}{\alpha}\frac{x}{x^2 + y^2} \tag{26}$$

and

$$v_s(x, y) = -\frac{m_i}{\alpha}\frac{y}{x^2 + y^2}, \tag{27}$$

where m_i is the flux of air into the exhaust slot, and u_s and v_s are the horizontal and vertical components of the air velocity, respectively, which result from the air flow into the slot.

2.2.3. *The air flow produced by the combination of the jet-induced and the sink flows*
Finally, the horizontal and vertical components of the air flow produced by the combination of the jet and the sink are given by

$$U(x, y) = u(x, y) - \frac{m_i}{\alpha}\frac{x}{x^2 + y^2}, \tag{28}$$

$$V(x, y) = v(x, y) - \frac{m_i}{\alpha}\frac{y}{x^2 + y^2} \tag{29}$$

in which $u(x, y)$ and $v(x, y)$ are given by Equations (11) and (12). The stream function ψ is then calculated by integration of the equation:

$$\frac{\partial\psi}{\partial y} = U(x, y), \tag{30}$$

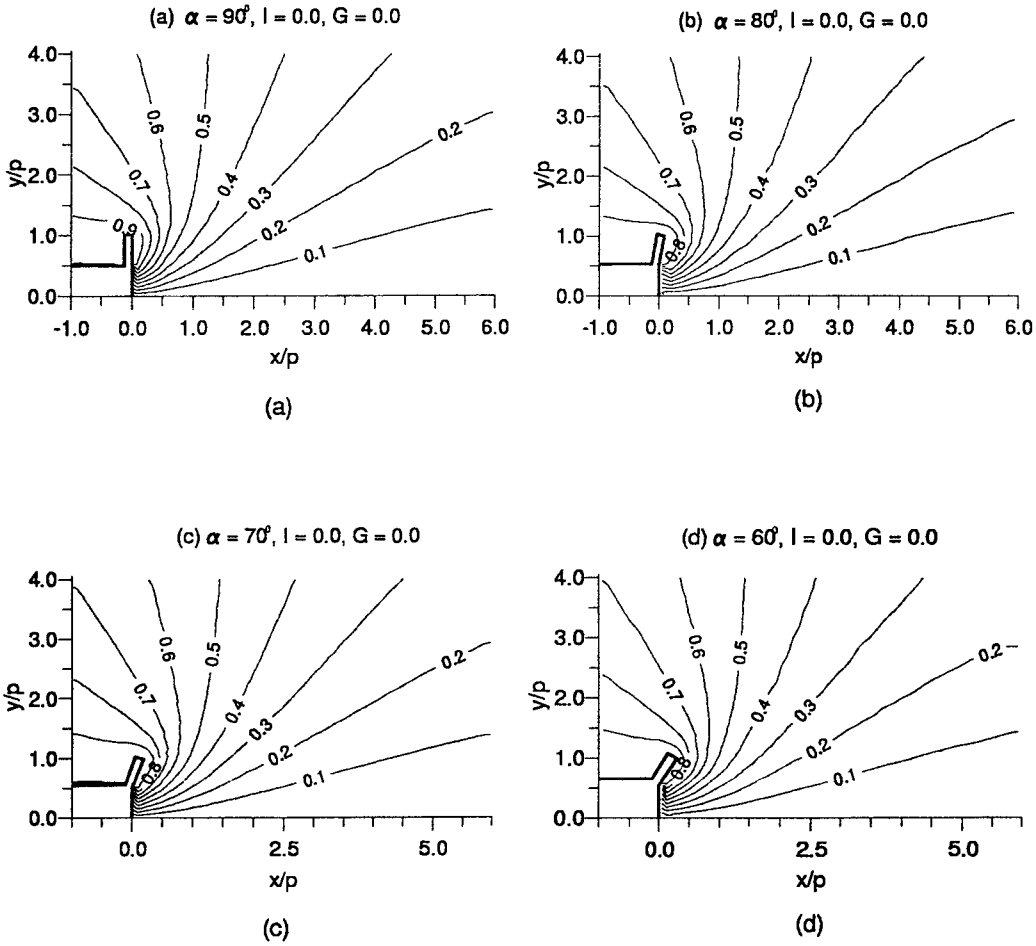

Figure 4. Streamlines for $u_j = 0{\cdot}0$ m/s, $u_i = 2{\cdot}0$ m/s, namely $I = 0{\cdot}0$, $G = 0{\cdot}0$, when (a) $\alpha = 90°$, (b) $\alpha = 80°$, (c) $\alpha = 70°$, and (d) $\alpha = 60°$, using the k-ϵ model.

subject to the condition that the stream function on the surface of the workbench is zero.

3. Results and discussion

The numerical calculations were performed for the Aaberg exhaust system which is similar to the workbench used in the experimental work by Hollis [19] when $\alpha = 90°$, $b = 0{\cdot}015$ m, $S = 0{\cdot}1$ m, $u_i = 2{\cdot}0$ m/s, $m_i = 0{\cdot}2$ m^2/s and for various values of m_j, where m_i and m_j are the fluxes per unit width. Further, we assume that for the turbulent free jet $C = 0{\cdot}31$ and we take $\alpha = 90°$, 80°, 70° and 60° with various jet velocities, u_j, ranging from 0 to 20·0 m/s. The numerical results are presented in terms of the momentum ratio I, which is defined by $I = \frac{u_j^2 b}{u_i^2 S}$, the operating parameter G, which is defined by $G = \frac{C u_j b^{1/2} p^{1/2}}{u_i S}$ and the streamline plots on which the stream function has been normalized by the flux of air m_i and therefore the line on which $\psi = 1{\cdot}0$ is the dividing streamline, *i.e.* the line which divides the air travelling into the exhaust slot from that entrained into the jet-induced flow. The lines of constant speed,

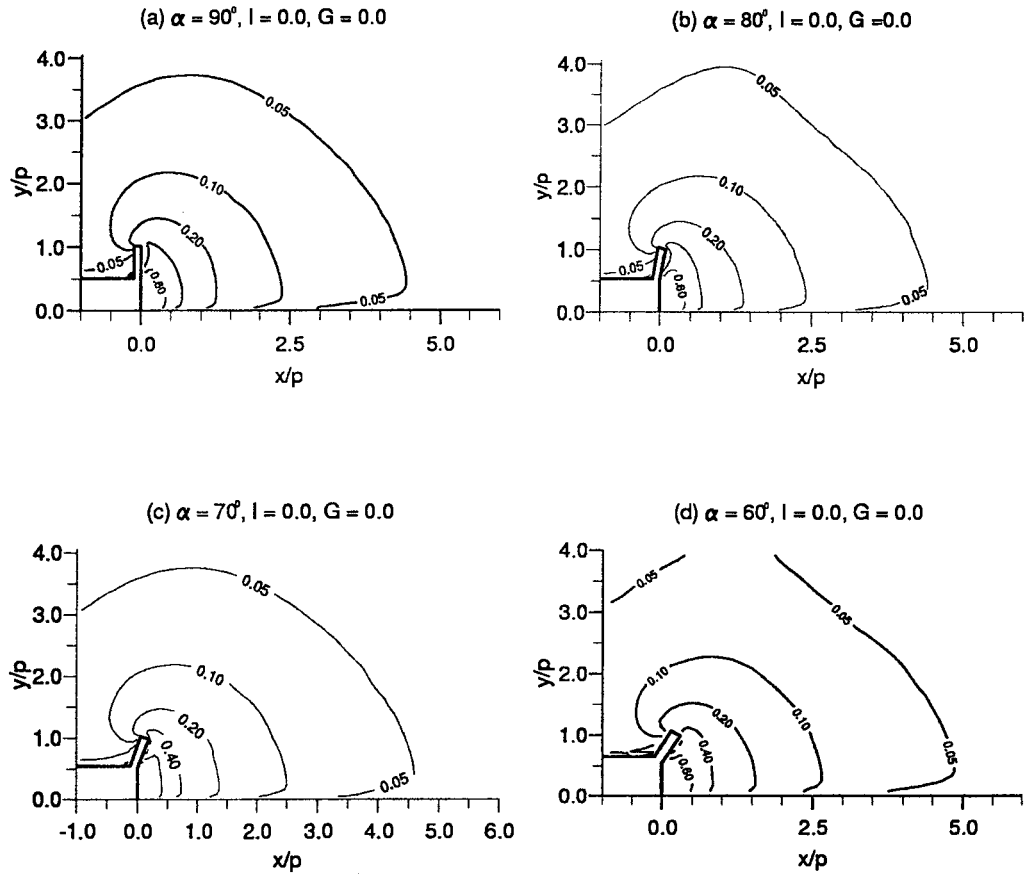

Figure 5. Non-dimensional lines of constant speed for $u_j = 0{\cdot}0$ m/s, $u_i = 2{\cdot}0$ m/s, namely $I = 0{\cdot}0$, $G = 0{\cdot}0$, when (a) $\alpha = 90°$, (b) $\alpha = 80°$, (c) $\alpha = 70°$, and (d) $\alpha = 60°$, using the k-ϵ model.

on which the air speed has been normalized by the air speed at the exhaust slot, are also used to reveal the effect of the jet flow on the air-velocity distribution.

When there is no jet flow, namely when $u_j = 0{\cdot}0$, this Aaberg exhaust hood becomes a conventional local exhaust hood. Figure 4 shows the streamlines created by the exhaust hood when $\alpha = 90°$, $80°$, $70°$ and $60°$ for the turbulent-flow model. It is observed that for the traditional local exhaust hood the effect of the angle of the flange on the movement of the air in the ventilated space is limited to a region close to the exhaust slot and the exhaust air flows towards the opening of the exhaust hood almost evenly from all directions. We observe that in front of the slot the contraction of the streamlines becomes stronger on decreasing the angle of the flange, but when the distance to the slot becomes large, then the effect of the angle on the streamlines becomes negligible. This is observed in Figure 4, which indicates that the streamline patterns are almost identical at large distances from the slot.

Figure 5 shows the non-dimensional lines of constant speed for the different angles α for the turbulent-flow model. It is clearly seen that the effect of the angle of the flange on the velocity distribution is limited to a very small region in front of the exhaust inlet and the air velocity decreases rapidly as the distance from the slot increases. Both Figures 4 and 5 indicate that the effect of the angle on the air-velocity distribution is limited to a very small distance, which is less than about p, from the slot.

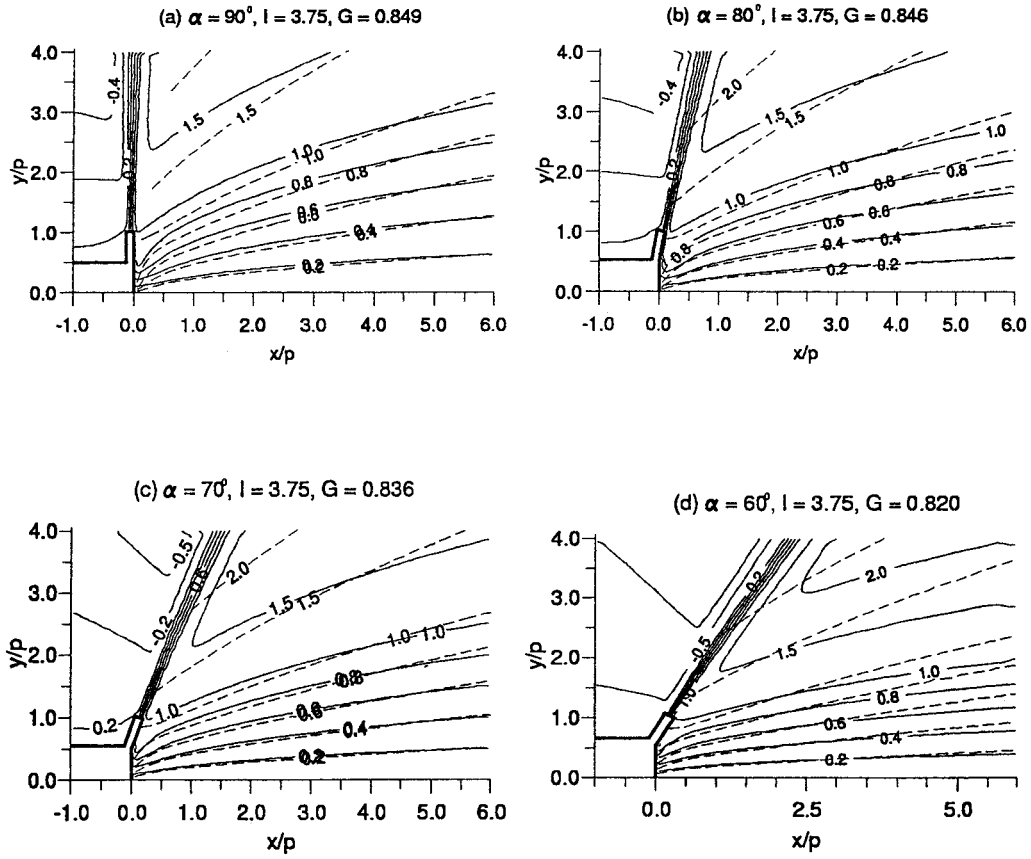

Figure 6. Streamlines for $u_j = 10{\cdot}0$ m/s, $u_i = 2{\cdot}0$ m/s, namely $I = 3{\cdot}75$, when (a) $\alpha = 90°$, (b) $\alpha = 80°$, (c) $\alpha = 70°$, and (d) $\alpha = 60°$. —— k - ϵ model, - - - - potential-flow model.

Figures 6, 7 and 8 show the streamlines of the air flow for jet angles of 90°, 80°, 70° and 60°, when $u_i = 2{\cdot}0$ m/s, $u_j = 10{\cdot}0$ m/s, $u_j = 15{\cdot}0$ m/s and $u_j = 20{\cdot}0$ m/s, namely, $I = 3{\cdot}75$, 8·44 and 15·0, respectively. Unlike the results shown in Figures 4 and 5, each of these figures show that the angle α has a significant effect on the whole air-flow field in the exhaust system. For a fixed value of the jet velocity u_j and the inlet velocity u_i the dividing streamline, *i.e.* the streamlines that divides the air exhausted to that which is not, becomes increasingly closer to the surface of the workbench as the angle of the jet decreases. As the plane of the jet flow turns towards the surface of the workbench, the dividing streamline is pushed closer to the surface of the workbench. Thus, the air velocity near the surface of the workbench increases, which is caused by both the flow towards the slot and the induced flow due to the jet. A decrease in the angle α decreases the area of the flow domain between the plane of the jet flow and the surface of the workbench. This decreases the area from where the air may be sucked into the exhaust slot and therefore in this region there is an increase in the air velocity towards the slot. The air velocity which is induced by the suction for a jet which is at an angle α increases by a factor which is approximately $90/\alpha$ compared with that when the jet angle is 90°.

In order to investigate the effect of the angle of the jet on the jet-induced flow, it is informative to investigate the simple situation when the inlet velocity is switched off, *i.e.* $u_i = 0{\cdot}0$, and u_j is fixed at 10 m/s, say. Figure 9 shows the ratio of the air velocity just outside the turbulent

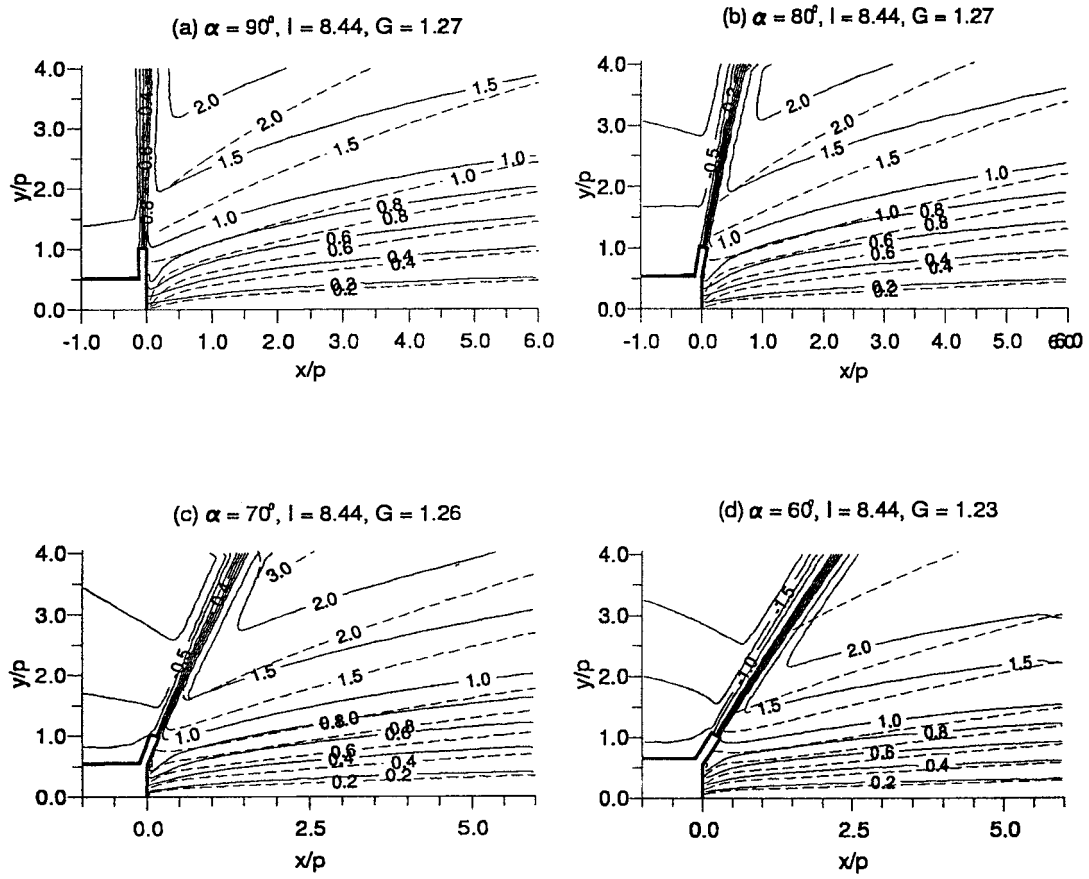

Figure 7. Streamlines for $u_j = 15{\cdot}0$ m/s, $u_i = 2{\cdot}0$ m/s, namely $I = 8{\cdot}44$, when (a) $\alpha = 90°$, (b) $\alpha = 80°$, (c) $\alpha = 70°$, and (d) $\alpha = 60°$. —— k-ϵ model, - - - - potential-flow model.

boundary layer on the workbench for $\alpha = 60°$, $70°$ and $80°$ compared to when $\alpha = 90°$. This figure reveals that in this situation, where there is a jet flow alone, for $x/p \gtrsim 1$ there is an increase in the air velocity near the surface of the workbench which is slightly less than the factor $90/\alpha$.

The increase in the air velocity due to the introduction of the jet flow over the whole physical domain is shown in the Figures 10–12 by the nondimensional lines of constant speed for $u_i = 2{\cdot}0$ m/s and $u_j = 10{\cdot}0$vm/s, $15{\cdot}0$ m/s and $20{\cdot}0$ m/s and for the angles $\alpha = 90°$, $80°$, $70°$ and $60°$, where the speed has been normalized by the inlet velocity u_i. Consistent with the phenomena shown for the streamline pattern in the Figures 6–8, we observe that there has been a significant increase in the air velocity and this has been achieved by decreasing the angle of the jet flow. Figures 10–12 show that the air velocity increases as the angle α decreases. This is because the thicknesses of the jet flow and the boundary layer on the surface of the workbench become relatively larger. We observe in all the Figures 6–8 and Figures 11–12 that there is very good global agreement between the results produced by the standard turbulent k-ϵ model and the potential model. The difference between the two models increases as the angle α decreases and the jet velocities increase; see for example Figures 10–12 when $\alpha = 60°$. This difference is due to the potential-flow model ignoring the existence of the thickness of both the jet and the boundary layer on the workbench. The smaller the angle

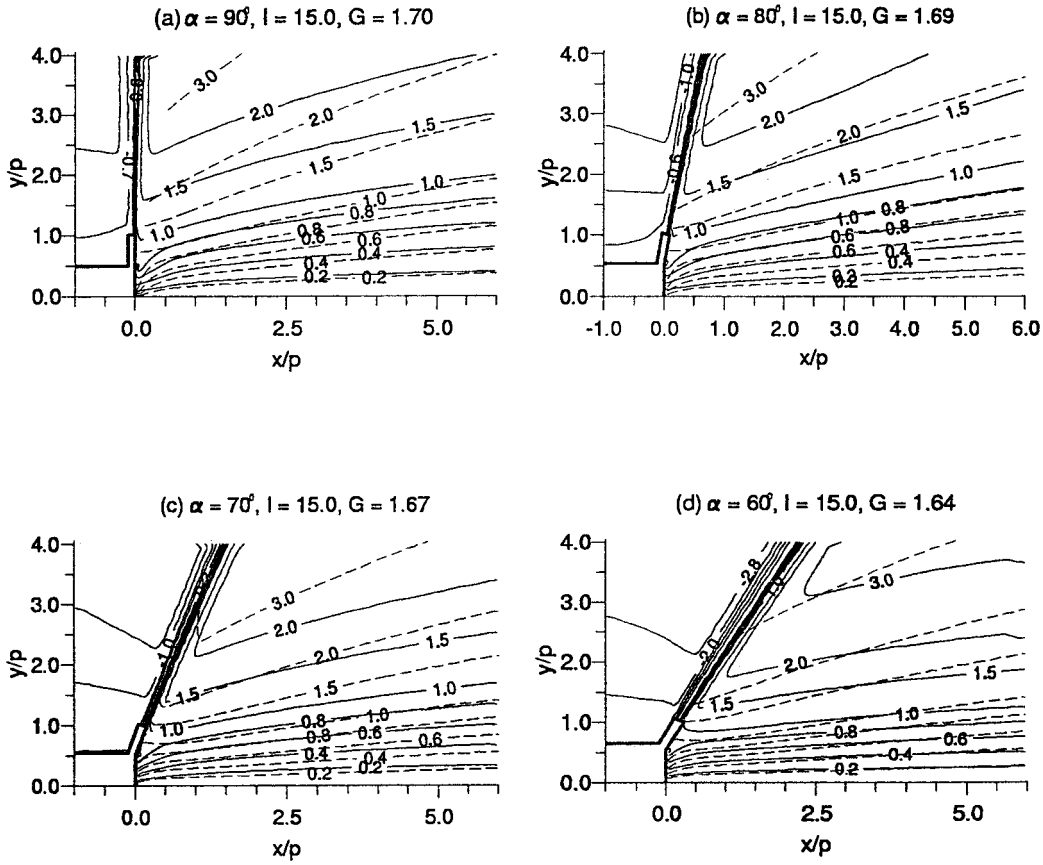

Figure 8. Streamlines for $u_j = 20{\cdot}0$ m/s, $u_i = 2{\cdot}0$ m/s, namely $I = 8{\cdot}44$, when (a) $\alpha = 90°$, (b) $\alpha = 80°$, (c) $\alpha = 70°$, and (d) $\alpha = 60°$. —— k-ϵ model, - - - - potential-flow model.

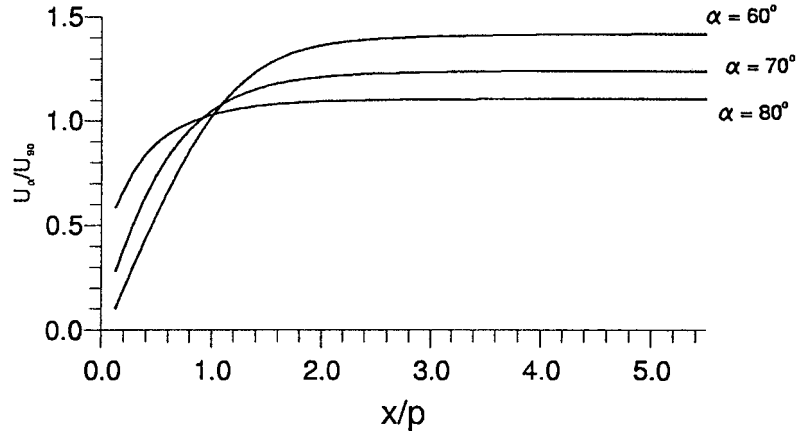

Figure 9. The ratio of the speed of the air just outside the turbulent boundary-layer when the angle of the jet is α to that when it is 90° when $u_j = 10$ m/s, $u_i = 0{\cdot}0$.

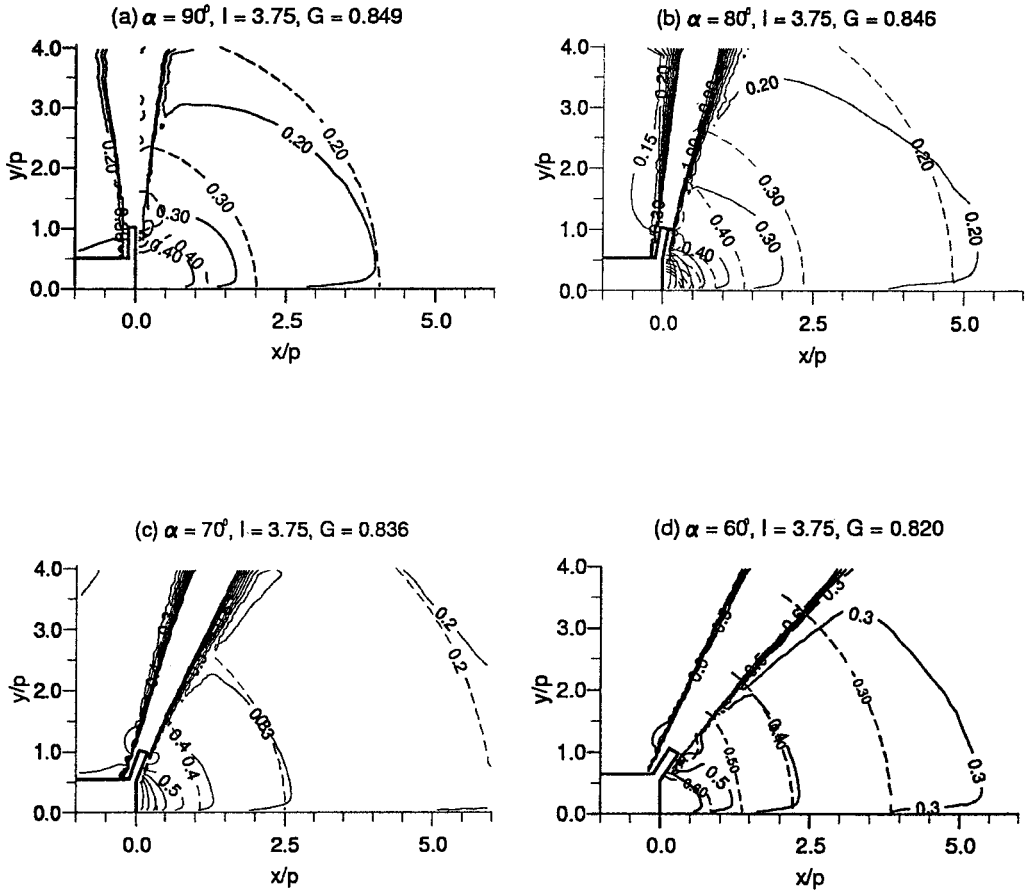

Figure 10. Non-dimensional lines of constant speed for $u_j = 10{\cdot}0$ m/s, $u_i = 2{\cdot}0$ m/s, namely $I = 3{\cdot}75$, when (a) $\alpha = 90°$, (b) $\alpha = 80°$, (c) $\alpha = 70°$, and (d) $\alpha = 60°$. —— k-ϵ model, - - - - potential-flow.

α and the jet velocities, the thicker are the jet and the boundary layer on the surface of the workbench and this significantly affects the air flow in front of the exhaust system.

Høgsted [1] and Fletcher and Saunders [4] observed that, if the air speed produced by the exhaust system becomes too small, then the contaminant cannot be drawn towards the exhaust slot because of the natural random background air movements that diffuse the air and the contaminant in every direction. A minimum capture speed for overcoming the effect of this random movement is required and this was found by Fletcher and Saunders [4] to be about 0·25 m/s. Therefore, the capture area is defined as an area that is bounded by the dividing streamline, the surface of the workbench and the line of constant speed, say 0·25 m/s, and the effective capture of the contaminant only takes place in this area. For the suction velocity $u_i = 2{\cdot}0$ m/s, Figure 13 shows the effect of the jet angle on the shape of the capture area produced when the jet velocity is 10·0 m/s, where both the potential and turbulent-flow models have been used. It is observed that decreasing the angle α significantly increases the length of the capture area along the surface of the workbench and this increases the size of the capture area. If we define L_{90} to be the length of the capture area along the surface of the workbench for the angle $\alpha = 90°$, then Figure 13 shows that the lengths of the capture area predicted by the potential model are $1{\cdot}19L_{90}$, $1{\cdot}47L_{90}$ and $1{\cdot}92L_{90}$ when $u_j = 10{\cdot}0$ m/s. Figure 13 also

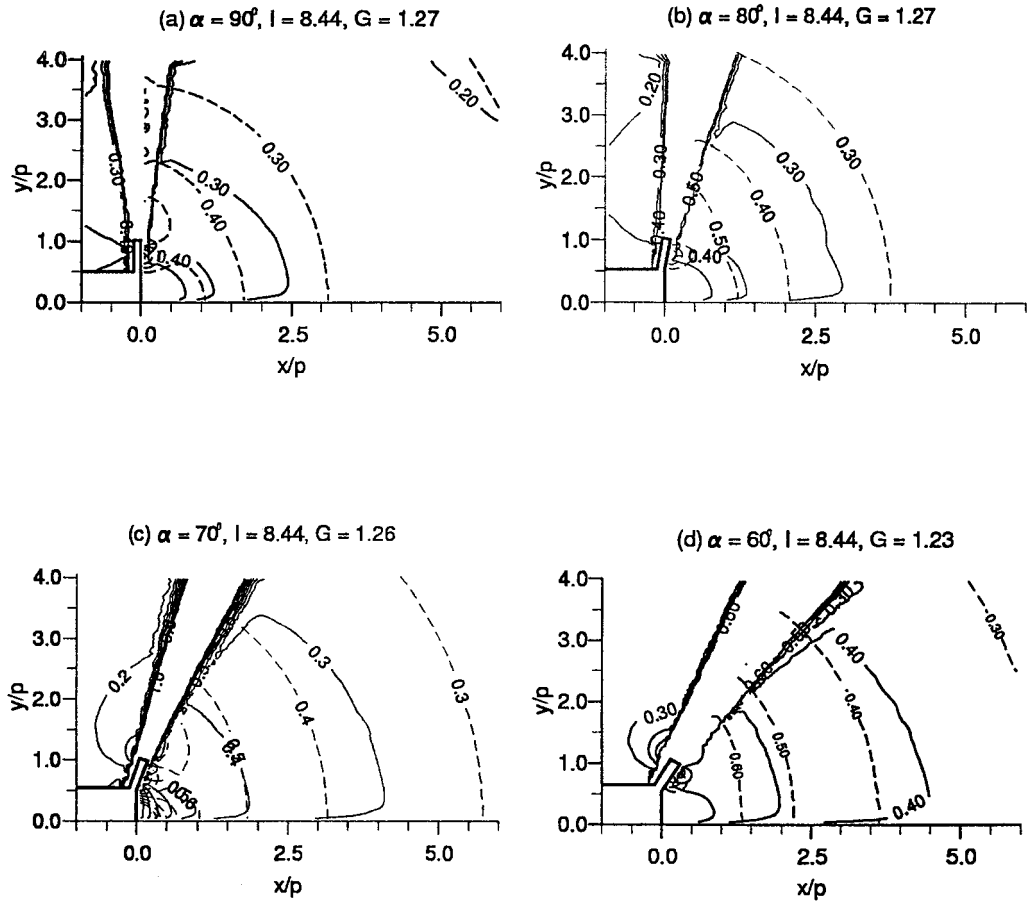

Figure 11. Non-dimensional lines of constant speed for $u_j = 15{\cdot}0$ m/s, $u_i = 2{\cdot}0$ m/s, namely $I = 8{\cdot}44$, when (a) $\alpha = 90°$, (b) $\alpha = 80°$, (c) $\alpha = 70°$, and (d) $\alpha = 60°$. ——- k-ϵ model, - - - - potential-flow.

shows that the length of the capture area predicted by the turbulent model is larger than that predicted by the potential model. This is because the turbulent air velocity in the region just outside of the boundary layer is higher than the air velocity predicted by the potential model and this is due to the existence of the boundary layer on the bench and the turbulent jet. These results reveal that the increase in the length of the capture area is slightly larger than the factor $90/\alpha$ and for the higher jet velocity this increase is larger.

It should be stressed that, when employing the standard turbulent k-ϵ model, the numerical calculations indicate that, for any angle α, the jet flow can be drawn into the exhaust slot if the jet velocity is too small. In general, in order to form the flow pattern shown in Figures 6–8, there is a minimum jet velocity u_j for a given inlet velocity u_i and this minimum jet velocity increases as the angle α decreases. Figure 14 shows the minimum momentum ratio $I_{\min}$ and minimum operating parameter $G_{\min}$ for different jet angles. It is observed that a smaller jet angle requires a larger momentum ratio or a larger operating parameter in order to avoid the jet flow being drawn into the exhaust slot.

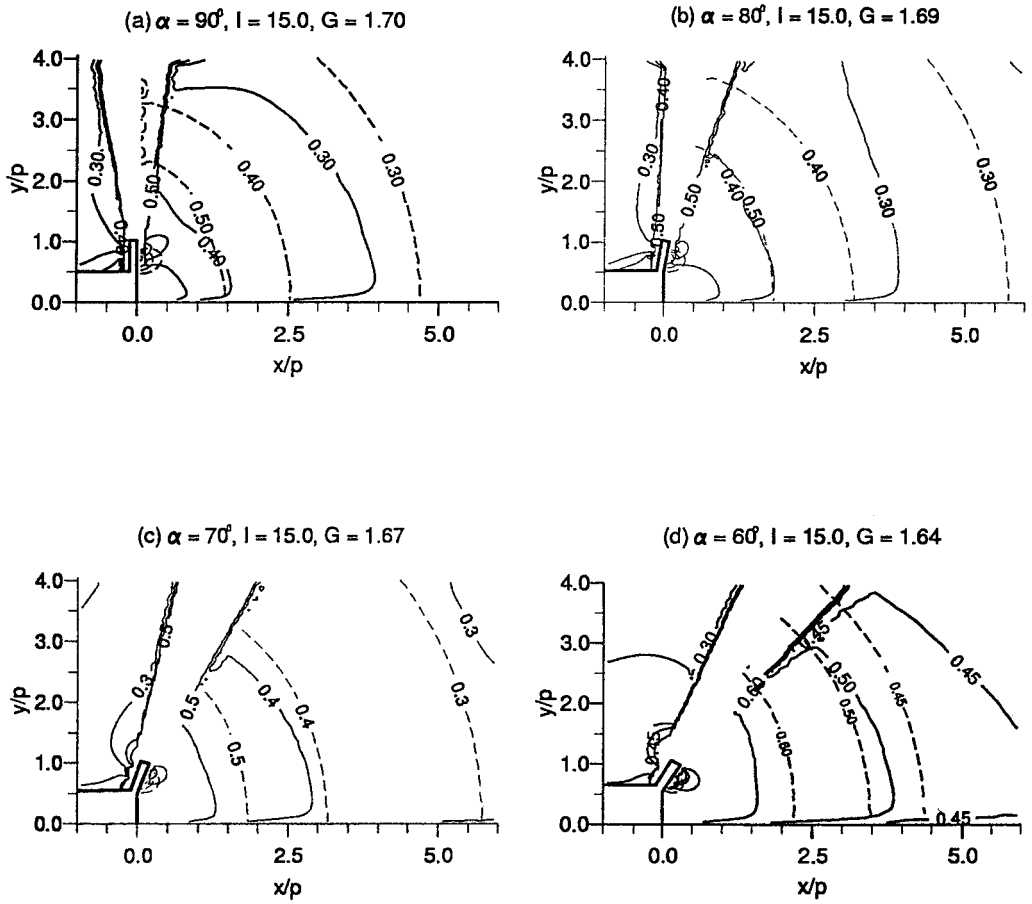

Figure 12. Non-dimensional lines of constant speed for $u_j = 20{\cdot}0$ m/s, $u_i = 2{\cdot}0$ m/s, namely $I = 15{\cdot}0$, when (a) $\alpha = 90°$, (b) $\alpha = 80°$, (c) $\alpha = 70°$, and (d) $\alpha = 60°$. —— k-ϵ model, - - - - potential-flow.

4. Conclusion

Both the standard k-ϵ and the potential flow models have been used to simulate the air flow in the two-dimensional bench version of the Aaberg exhaust system with an inclined free jet and results have been obtained for jet angles $\alpha = 90°$, $80°$, $70°$ and $60°$. The results obtained

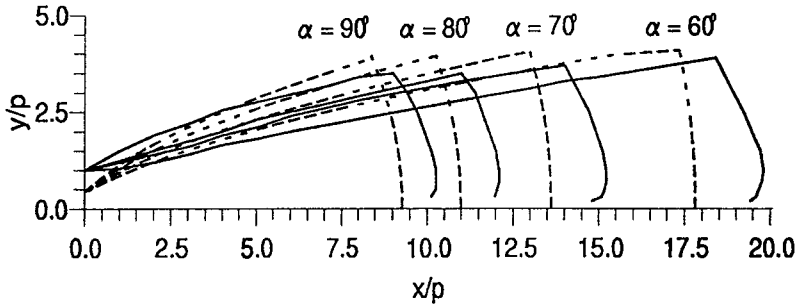

Figure 13. Capture area when $u_i = 2{\cdot}0$ m/s, $u_j = 10{\cdot}0$ m/s, for $\alpha = 90°$, $80°$, $70°$ and $60°$. —— k-ϵ model, - - - - potential-flow.

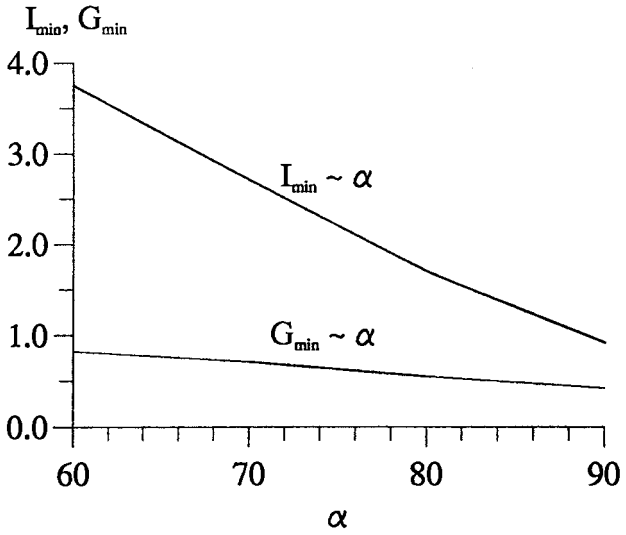

Figure 14. The minimum momentum ratio and operating parameters for different jet angles.

from both the potential and the turbulent-fluid models reveal that, on decreasing the angle α, the air speed along the surface of the workbench increases. All the numerical results show the following for the same operational power of the exhaust system: the smaller the angle α that the jet makes with the direction of the exhaust system, the closer to the surface of the workbench is the separating streamline. This leads to a higher air velocity near the surface of the workbench, *i.e.* in the vicinity where the contaminant is produced. The numerically predicted results for the effective capture region indicate that the capture distance for a jet at an angle α compared with that for the angle 90° increases by a factor that is greater than $90/\alpha$ and the value of this factor increases as the jet velocity increases. However, it should be stressed that at a fixed angle α there exists a critical momentum ratio, or a critical velocity, under which the jet flow collapses and forms a short circuit. In the other words, for a fixed momentum ratio there exists a critical angle below which the air flow starts to short-circuit.

From the results presented in this paper we conclude that a significant enhancement of the air speed near the surface of the workbench can be achieved by increasing the power of the jet flow, or using a smaller angle α. The advantage of using an inclined jet flow is that, for the same degree in the enhancement in the air velocity, the required power of the jet can be reduced. Therefore, both the cost of operating the exhaust system and the noise can be reduced.

In this paper we have validated a simple potential model by comparing the results obtained with those obtained using the full k-ϵ model. Now we need to optimise the operational parameters and the geometry of the Aaberg system, including the angle α of the jet, so that the equipment is more energy efficient. In order to do this we need to investigate experimentally the jet angles α that are less than 90° but do not encounter situations where the jet is entrained into the exhaust slot. Thus, the turbulent k-ϵ model should be validated against this new experimental data. Once this has been performed, the computational technique can be used to give practical guidelines for the most efficient use of the Aaberg system.

Acknowledgements

The authors would like to thank the EPSRC for the financial support of this work.

References

1. P. Høgsted, Air movements controlled by means of exhaustion. In: T. G. Malmstrom (ed.), *ROOMVENT'87. Int. Conf. on Air Distribution in Ventilated Spaces*, Stockholm (1987).
2. C. E. Hyldgard, Aerodynamic control of exhaust. In: T. G. Malmstrom (ed.), *ROOMVENT'87. Int. Conf. on Air Distribution in Ventilated Spaces*, Stockholm (1987).
3. L. G. Pedersen and P. V. Nielsen, Exhaust system reinforced by jet flow. In: D. T. Grimsrud (ed.), *ROOMVENT'91. Int. Conf. on Air Distribution in Ventilated Spaces*, Cincinnati, Ohio (1991).
4. B. Fletcher and C. J. Saunders, Private communication between G. R. Hunt and D. B. Ingham and the Health and Safety Executive, Research Division, Sheffield, England (1991).
5. B. Fletcher and C. J. Saunders, Jet enhanced local exhaust ventilation. *The Annals of Occupational Hygiene* 37 (1993) 15–24.
6. R. Braconnier, D. Thiebaut, G. Aubertin, J. C. Serieys and J. P. Muller, Double-flow devices for the capture of contaminants. In: H. D. Goodfellow (ed.), *Proc. of 3rd Int. Symp. on Ventilation for Contaminant Control*, Chemical Engineering Monographs, Elsevier 24 (1986) pp. 743–753.
7. L. G. Pedersen, *REEXS-Reinforced Exhaust System*, Ph.D Thesis, Danish Technological Institute, Demark (1991) 214 pp.
8. P. Sprecher and R. Weber, Local exhaust ventilation with REEXS. In: R. Niemela, J. Railio, E Sundquist and E Tahti (ed.), *Ventilation 2000. 6th International Symposium on Ventilation for Contaminant Control*, Finnish Institute of Occupational Health, Helsinki 1 (2000) pp. 39–42.
9. G. R. Hunt and D. B. Ingham, The fluid mechanics of a two-dimensional Aaberg exhaust hood. *The Annals of Occupational Hygiene* 36 (1992) 455–476.
10. G. R. Hunt and D. B. Ingham, Long range exhaustion - A mathematical model for the axisymmetric air flow of a local exhaust ventilation hood assisted by a turbulent radial jet. *The Annals of Occupational Hygiene* 40 (1996) 171–196.
11. G. R. Hunt, *The fluid mechanics of the Aaberg exhaust Hood*, Ph.D Thesis, The University of Leeds, Leeds, United Kingdom (1994) 234 pp.
12. G. R. Hunt and D. B. Ingham, A mathematical model of the fluid-flow of a slot exhaust hood reinforced by a two-dimensional jet-flow. *Math. Engng. Ind.* 4 (1993) 227–247.
13. X. Wen and D. B. Ingham, Theoretical and numerical predictions of two-dimensional Aaberg slot exhaust. *The Annals of Occupational Hygiene* 44 (2000) 375–390.
14. X. Wen, G. R. Hunt and D. B. Ingham, A boundary integral technique for the numerical modelling of the air flow for the Aaberg exhaust system. *Engineering Analysis with Boundary Elements* 24 (2000) 477–484.
15. G. R. Hunt, X. Wen and D. B. Ingham, Jet assisted local exhaust ventilation – The effect of jet direction, In: T. G. Malmstrom (ed.), *Proc. of Roomvent 2000. 7th International Conference on Air Distribution in Rooms*, Stockholm (2000) pp. 669–674.
16. X. Wen and D. B. Ingham, The air flow of two-dimensional Aaberg slot exhaust Hoods. In: R. Niemela, J. Railio, E Sundquist and E Tahti (eds.), *Ventilation 2000. 6th Int. Conf. on Ventilation for Contaminant Control*, Finnish Institute of Occupational Health, Helsinki 1 (2000) pp. 121–123.
17. D. Gubler and A. Moser, Tuning of a reinforced extract system by computational fluid dynamics. In: R. Niemela, J. Railio, E Sundquist and E Tahti (eds.), *Ventilation 2000. 6th Int. Conf. on Ventilation for Contaminant Control*, Finnish Institute of Occupational Health, Helsinki 1 (2000) pp. 104–107.
18. B. E. Launder and D. B. Spalding, The numerical computation of turbulent flows. *Comp. Methods Appl. Mech. Engng.* 3 (1974) 269–289.
19. E. J. Hollis, Investigation of an Aaberg Workbench, Health and Safety Executive, Research Division, Sheffield, England, HSL Project Report IR/I/VE/95/2 (1995) 32 pp.
20. S. V. Patankar, *Numerical Heat Transfer and Fluid Flow*. Washington, DC: Hemisphere (1980) 197 pp.